Interfacial modification by lithiophilic oxide facilitating uniform and thin solid electrolyte interphase towards stable lithium metal anodes

Lu, L; Pei, Yutao T.

Published in:
Materials Today Energy

DOI:
10.1016/j.mtener.2021.100748

Publication date:
2021

Materials Today Energy 21 (2021) 100748

Contents lists available at ScienceDirect

Materials Today Energy

journal homepage: www.journals.elsevier.com/materials-today-energy/

Interfacial modification by lithiophilic oxide facilitating uniform and thin solid electrolyte interphase towards stable lithium metal anodes

L.Q. Lu*, Y.T. Pei

Advanced Production Engineering, Engineering and Technology Institute Groningen, Faculty of Science and Engineering, University of Groningen, Nijenborgh 4, 9747 AG, Groningen, the Netherlands

ARTICLE INFO

Article history:
Received 14 January 2021
Received in revised form
2 April 2021
Accepted 3 April 2021
Available online 15 April 2021

Keywords:
Lithium metal batteries
Lithiophilic oxide surface
SEI film
Dendrites
Li_2O

ABSTRACT

In this work, metal foam current collectors (CCs, i.e. nickel [Ni] and copper [Cu]) were treated by thermal oxidation to create a lithiophilic oxide surface that exhibited enhanced electrochemical performances of lithium anodes such as the cyclic stability of Coulombic efficiency at different current densities for various capacities compared to pristine CCs. The oxidized CCs facilitated much increased diffusivities of ions for lithium growth than pristine CCs. It was found that an inhomogeneous solid electrolyte interphase (SEI) formed on pristine CCs while a uniform SEI formed on oxidized CCs. Uniform lithium (Li) deposition can be achieved on oxidized CCs owing to the lithiophilic oxide surface containing metal nanoparticles and the ionic compound lithium oxide (Li_2O) matrix that led to a uniform SEI film and many nucleation sites. In addition, the porous and non-porous composite anodes exhibited different electrochemical performances. The porous composite anodes showed initial lower voltage hysteresis but shorter lifetime with carbonate-based electrolyte than non-porous composite anodes. The porous composite anodes showed better rate performances in full-cell measurements while the non-porous composite anodes displayed better stability. The interfacial modification of porous hosts by lithiated oxides and the effects of porous structure on battery performances can be also useful for designing other electrodes (e.g. sodium [Na], potassium [K], zinc [Zn]).

1. Introduction

As an integral part of global clean energy transition, batteries play an essential role in future low-carbon energy applications and management. The increasing demand for clean and renewable energy is powering the need for batteries. As a result, developing high-energy-density and high-performance batteries is attracting great attentions particularly to meet the increasing demands of societal needs such as electric transportations and power grids [1,2]. As the one having the lowest standard electrode potential (−3.04 V vs. standard hydrogen electrode) and lightest metal (0.534 g/cm^3), lithium (Li) metal owns a high theoretical specific capacity (3860 mA h/g) and volumetric capacity (2061 mA h/cm^3) that are much larger than those of conventional graphite anodes [3]. However, the commercialization of rechargeable Li metal batteries have been impeded by a number of issues from Li anodes such as the inferior cyclic stability, low Coulombic efficiency (CE) and severe safety concerns [3,4]. These diminished performances and safety issues mainly stem from the growth of Li dendrites during electrochemical deposition of Li, infinite volume change, repeated break and formation of solid electrolyte interphase (SEI) films, and formation of dead lithium debris during deposition and stripping processes of lithium [3–5].

To tackle the abovementioned problems, storing lithium in an electrically conductive porous framework provides an effective strategy [4,5]. First, the porous structure can suppress the dendritic growth by reducing the local current density or confine the dendrites within the electrodes [6]. Second, the electrical skeleton can facilitate the electron transport. Third, the pores provide more channels for the transport of lithium ions and thus could improve the rate performances. Fourth, well sealing of lithium in porous hosts can prohibit direct contact between lithium and the electrolyte, stabilizing SEI films and improving the CE [7]. In addition, the encapsulation of lithium in the porous structure can also restrain the volume change of Li electrodes during discharge and charge [8]. These aspects of porous hosts bring forth higher CE, better cyclic performances and safety. In particular, metallic

* Corresponding author.
E-mail address: ewan.lu@rug.nl (L.Q. Lu).

https://doi.org/10.1016/j.mtener.2021.100748

scaffolds such as porous copper and porous nickel have many advantages such as high specific surface area, good strength and stiffness, and high conductivities [9].

However, there are still some challenges in solving the above-mentioned issues to commercialize Li-metal anodes and in the synthesis of composite anodes. Stabilizing and manipulating the SEI to suppress the growth of dendrites and improve CE provide guidelines [10–14]. Although progresses have been made on revealing the composition, microstructures, formation processes, and functions of the inorganic compounds of SEI films [15–22], it still requires more efforts on further uncovering the mysteries of SEI films, such as the influencing factors (e.g. surface geometry, chemical compositions, etc.) on the SEI formation and their consequences on the growth behavior of Li and electrode performances. Regarding the synthesis of composite anodes, commonly a lithiophilic surface of host materials is of extremely significance for electrode synthesis by thermal infusion of Li or electroplating to achieve uniform loadings, storing lithium by creating nucleation sites, and decreasing the nucleation/reaction energy barrier [23]. A number of strategies have been employed such as chemical synthesis/deposition of various kinds of metal oxide coatings on lithiophobic copper or nickel current collectors such as ZnO [24–27], fluorides [28], metals that can form alloys with Li [23,29,30], carbon coatings that guide the deposition of dendrite-free lithium [31–33]. However, understanding these modifications such as the commonly employed oxides on the SEI formation is still limited. Previous work showed that lithium has good wetting properties on lithium compounds (e.g. lithium nitride [Li_3N], oxide [Li_2O], and carbonate [Li_2CO_3]) [34]. In particular, a rather low energy is required for molten lithium wetting on lithium oxide, indicating it as a possible media for thermal-infusion synthesis and tuning the plating and stripping of lithium.

When designing composite anodes, the capacity of cathodes, active lithium and non-reversible lithium consumed by the SEI and dead lithium need to be taken into account for determining an optimal lithium loading. The composite anodes can be made porous or non-porous. For most of the reported composite Li anodes synthesized by infusion of porous metals with molten lithium, usually their pores are completely filled with lithium [6,24,30,35–37], while the loadings of lithium are much excessive. In addition, it still lacks studies on how the porosity affects the electrochemical performances of the composite anodes for lithium-metal and lithium-sulfur (Li–S) batteries. To evaluate the effect of a non-porous structure (saturated with Li) and porous structure (with reduced Li content) on the electrode and full-cell performances could be meaningful for designing Li metal batteries. To the best of our knowledge, it is still elusive on how the porous structure influences the capacity, cyclic performances, rate performances and electrochemical deposition and stripping behaviors of lithium for applications of lithium-metal and lithium-sulfur batteries.

Herein, we investigated the influences of the surface modification of current collectors (CCs) by a lithiophilic oxide coating on the formation of solid electrolyte interphase (SEI), and electrochemical performances. The oxidized porous current collectors (e.g. oxidized Ni foam, named as ONiF) comprised a nanostructured coating containing a nanoporous metal (e.g. nickel [Ni]) framework embedded in a lithium oxide (Li_2O) matrix after thermal infusion of lithium or electrochemical lithiation. The oxide-modified current collector exhibited excellent Coulombic efficiency (CE) stability at different current densities. The plating behaviors of Li and SEI formation on the modified current collectors and pristine current collectors were further scrutinized by electron microscopy and electrochemical impedance spectroscopy (EIS). In addition, the effects of the structure of composite anodes on the electrochemical performances were investigated. Two composites that were macroporous one with 20 wt% of Li (named as 20%Li@ONiF) and non-porous one with 56% (named as 56%Li@ONiF) were synthesized. The lithium plating and stripping behaviors, microstructures after testing, and full-cell performances paired with $Li_4Ti_5O_{12}$ (LTO) and sulfur cathodes of the two composite anodes demonstrated that the porous and non-porous anodes exhibit much different electrochemical performances. The non-porous anodes surpassed macroporous anodes in terms of the long-term stability and capacities in particularly for Li–S batteries.

2. Results and discussion

2.1. Lithiophilic oxide coating and composite anodes

Fig. 1 schematically illustrates the facile synthesis process of composite anodes, including the thermal oxidation of current collectors (e.g. Ni foam), thermal infusion of molten Li and controlling the loading and content of Li in the composite anodes. Due to the poor wettability of molten Li on current collectors, it was difficult to infuse lithium into pristine Ni foam (see video 1 in the Supplementary). In contrast, the oxide coating has good affinity to lithium and facilitates fast and uniform infusion of Li into the surface-oxidized current collectors (only took several seconds, see video 2 in the Supplementary). Fig. 2 reveals the microstructure of the thermal oxidization coating using scanning electron microscopy (SEM). The current collector made of commercial Ni foam has a three-dimensional macroporous structure and hollow ligaments with voids of around 30 μm (Fig. 2a and b). After oxidation, an oxide coating composed of nanoparticles uniformly and entirely formed on the outside and inside surfaces of the ligaments as supported by the microstructural analyses and EDS element mappings (Fig. 2c–h). The oxide coating has a thickness of around 200 nm as shown in Fig. 2c and e. The content of Li could be easily and precisely adjusted by adding the amount of molten lithium, which was more controllable and reproducible than tuning the infusion time.

Two different electrode structures by varying lithium contents were prepared, which were the porous composite anodes (20% Li@ONiF) and non-porous anodes (56%Li@ONiF). As shown in Fig. 3a, the large pores of 20%Li@ONiF anodes kept similar to those of the original Ni foam. However, the hollow ligaments were fully filled with lithium from the observation of the fractured cross sections as seen in Fig. 3b. Lots of dispersed Ni nanoparticles were formed as a result of the redox reaction between the oxide coating and molten Li (Fig. 3c and d, Fig. S1 in the Supplementary). The Li_2O matrix was actually embedded in a metallic nanoporous framework because of the Li insertion [38], which can be observed by etching/washing away the Li and Li_2O by water (Fig. S2). Although Li_2O is electrically insulating, the implanted metallic nanoporous framework could improve the electrical conductivity and ionic conductivity using nanosized Li_2O [39]. The external surface of 20% Li@ONiF was entirely covered by a lithium coating with a thickness of 2–3 μm (Fig. 3c and element mappings in Fig. S3). Thus, it can be seen that molten Li preferentially infused into the voids of the ligaments due to the capillary effect, demonstrating the good affinity of the lithiophilic oxidized surface. In contrast, all the pores of non-porous 56%Li@ONiF anodes were fully filled with lithium, which can be seen from the surface and cross section of the anodes (Fig. 3e–f and Fig. S4).

2.2. Lithium growth on oxide-modified current collectors and electrochemical performances

The growth behavior of Li on the oxide-modified and pristine metallic surfaces in carbonate electrolyte was investigated. First, the nucleation and growth of lithium on the surfaces of

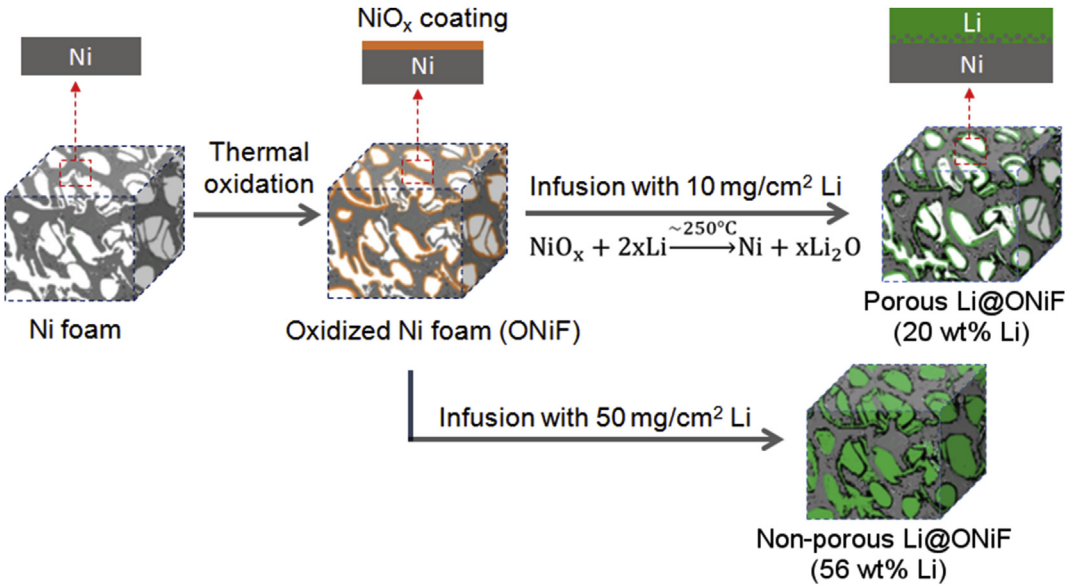

Fig. 1. Schematic illustration of the synthesis process of Li@ONiF, including thermal oxidation and infusion of ONiF with molten lithium.

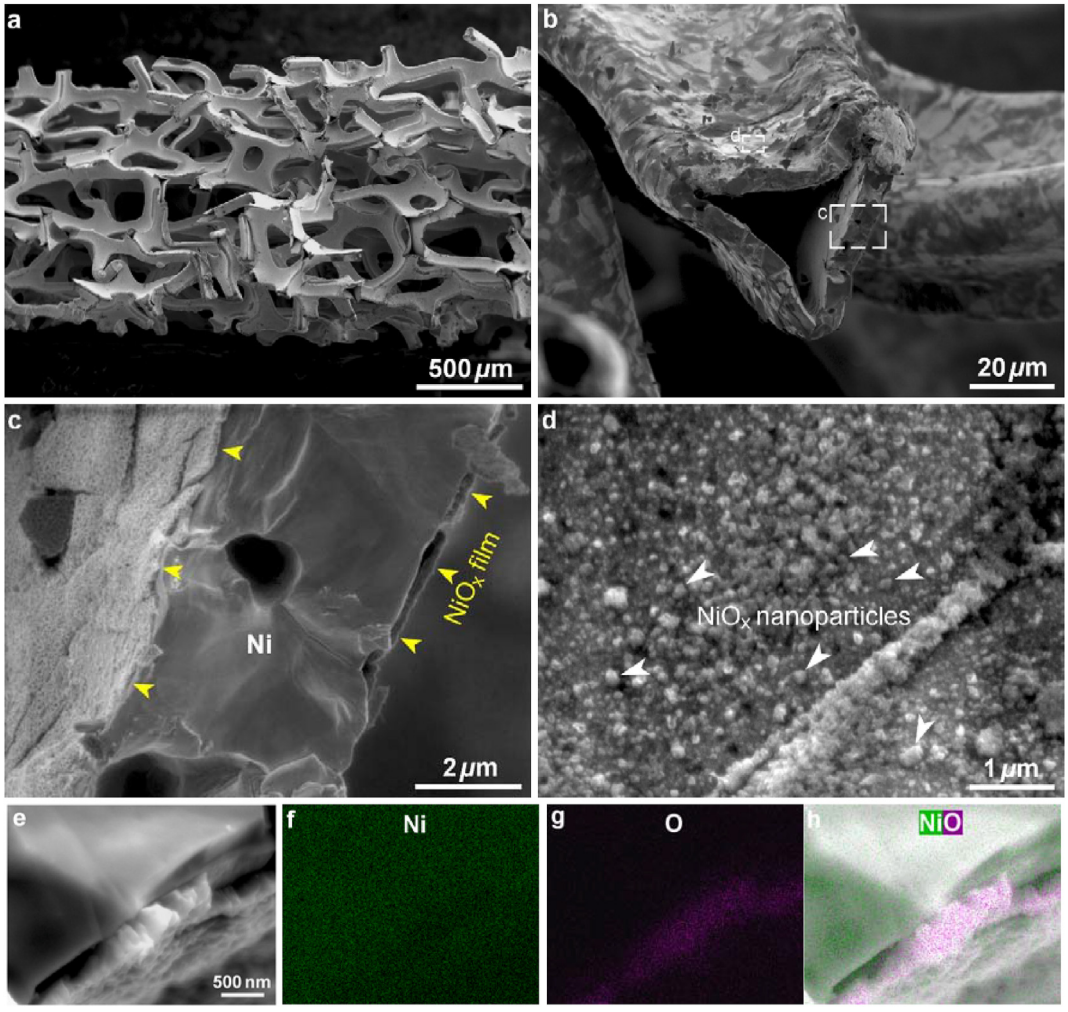

Fig. 2. Microstructure of oxidized 3D Ni foam (ONiF): (a) overview, (b, c) fractured ONiF ligament revealing the nickel oxide film (NiO_x) ~ 200 nm thick, and (d) close view of NiO_x film grown on the surface of Ni foam. (e–h) SEM image of the cross section and EDS mapping of O, Ni and the overlay.

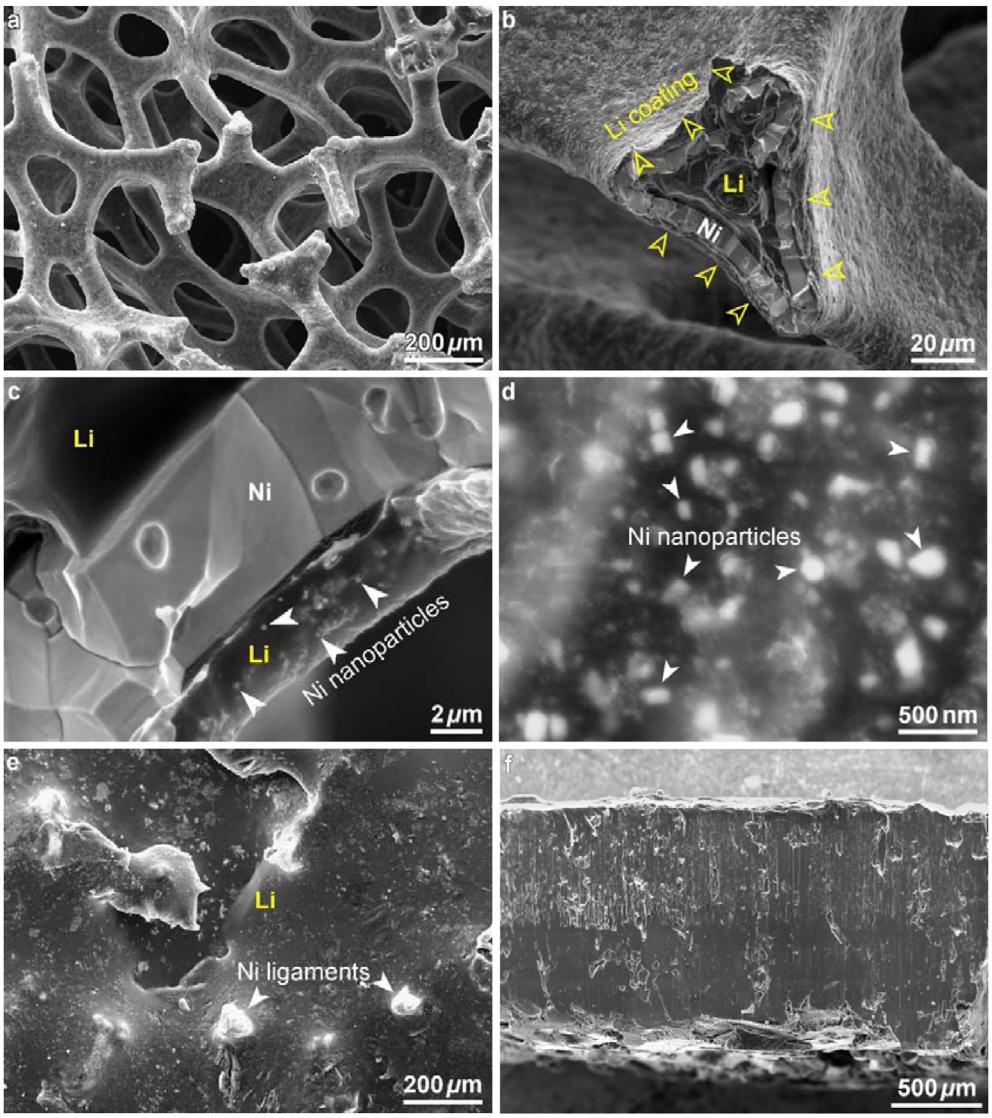

Fig. 3. Microstructures of porous 20%Li@ONiF anode (Li loading ~10 mg/cm^2): (a) overview, (b) fractured Ni ligament, (c) Li coating formed on the outer surface of hollow Ni ligament, and (d) close view of Li coating embedded with Ni nanoparticles. Microstructures of non-porous 56%Li@ONiF anode (Li loading ~50 mg/cm^2): (e) top view and (f) fractured cross section.

the oxidized nickel foam (ONiF) lithiated beforehand and Ni foams were investigated. Fig. 4a shows there were no obvious needlelike Li formed on the ONiF lithiated beforehand. Instead, many mossy-like lithium domains with a size of several microns can be observed (Fig. 4b). In contrast, for the pure Ni foam there were lots of thick and long whiskers grown on the ligaments (Fig. 4c). The differences in the growth behavior indicated that the surface of ONiF lithiated beforehand was in favor of homogeneous lithium plating. Mossy-like Li domains were also found on ONiF electrochemically lithiated beforehand (Fig. S5). The voltage profiles (Fig. 4d) illustrated that the growth of Li on ONiF lithiated beforehand had much lower nucleation overpotential than that on the non-oxidized Ni foams, demonstrating a lower energy barrier of nucleation for Li on ONiF. It can be ascribed to the oxide coating that provided many nucleation sites. The growth of Li on ONiF electrochemically lithiated beforehand (galvanostatic discharge/charge between 0.001 and 1.0 V) also exhibited lower mass-transport overpotential than that on the non-oxidized surfaces, which can be originated by the SEI films.

The electrochemical impedance spectroscopy (EIS) was carried out to compare the growth kinetics of Li onto the oxide coating and pristine metallic surfaces. As shown in Fig. 4e, it was revealed that the lithiated ONiF had much lower charge-transfer resistances than that for the pristine Ni foams, implying a higher reaction rate for lithium growth on ONiF. By plotting the real part of impedance (Z') as a function of the reciprocal root square of the angular frequencies ($\omega^{-0.5}$) in the low-frequency region, the Warburg coefficient σ can thus be obtained by the slope of the linear plots (Fig. 4f). It showed that the Warburg coefficient was much reduced for oxidation-treated electrodes in contrast to that of pristine electrodes (13 vs. 94 Ω/s$^{0.5}$). The ionic diffusivity (D) referred to the following equation [40]:

$$D = 0.5\left(\frac{RT}{An^2F^2\sigma C}\right)^2 \quad (1)$$

where R is the gas constant, T is the temperature (298.5 K), A is the area of the electrode surface, n is the number of electrons involved, F is Faraday's constant, and C is the molar concentration of Li^+ in the electrolyte. Because ONiF and non-oxidized Ni foam had almost the same area A, thus Eq. (1) can be simplified as $D \sim 1/(\sigma)^2$. It gets

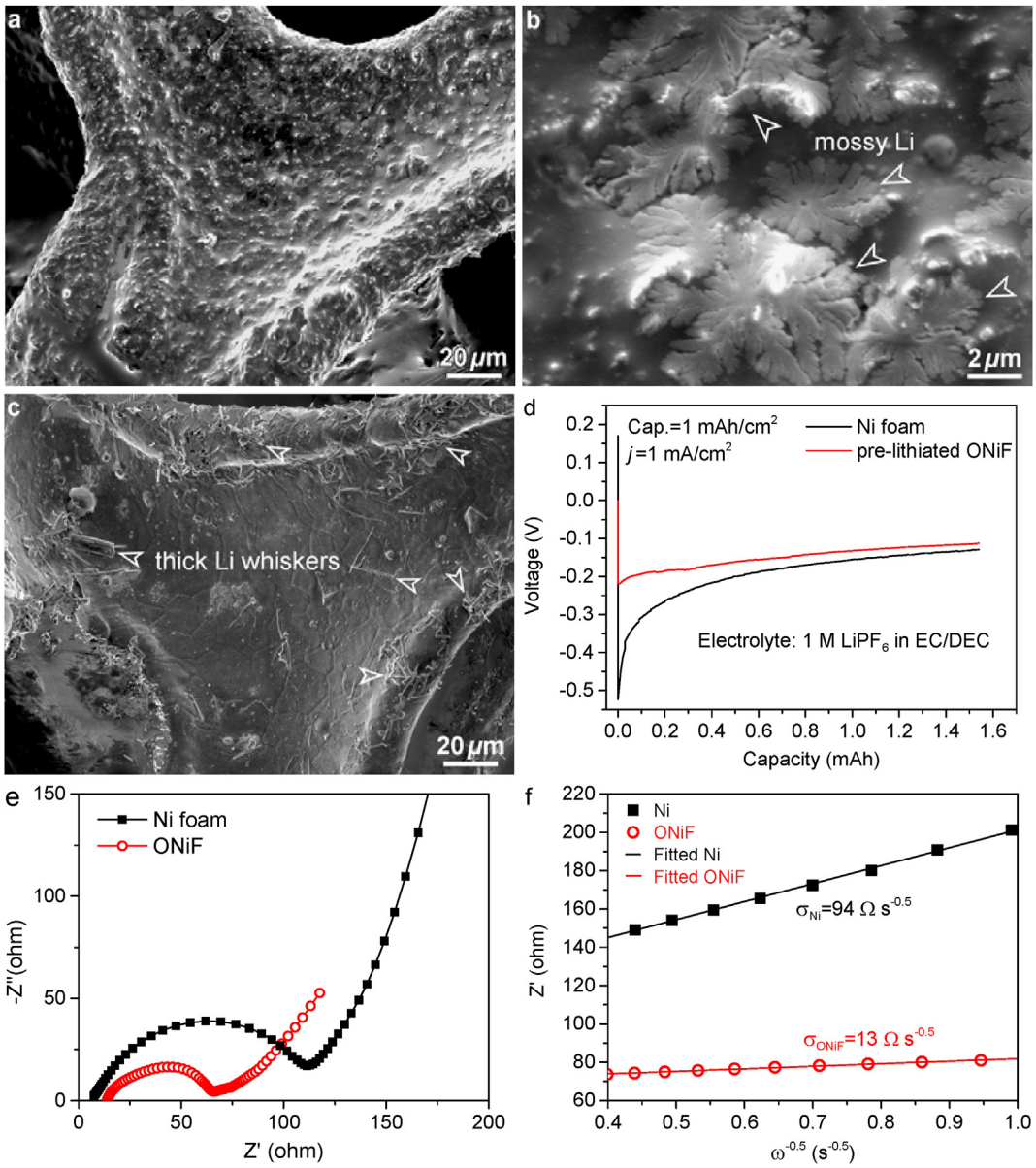

Fig. 4. Growth of Li on ONiF thermally lithiated beforehand (a–b) and non-oxidized Ni foam (c) under a current density of 1 mA/cm^2 for a total of 1 mA h/cm^2 of Li. (d) Voltage profile of Li deposition (1 mA h/cm^2) onto Ni foam and electrochemically lithiated ONiF at 1 mA/cm^2; (e) Nyquist plots of cells with using lithiated ONiF and lithiated Ni foam before deposition of Li, (f) the relationship between Z′ and $\omega^{-0.5}$ at low frequencies.

$$\frac{D_{ONiF}}{D_{Ni}} = \left(\frac{\sigma_{Ni}}{\sigma_{ONiF}}\right)^2 = 52 \quad (2)$$

It can be seen that the diffusivity of Li ions for Li nucleation on oxidation-treated electrodes increases significantly (52 times) compared with pristine metallic electrodes. As it is known that the diffusivity of ions is a significant factor for the transition of lithium growth from root growth to tip growth [41], the enhanced diffusivity with using oxidation treated electrodes can be the main reason for the reduced mass-transport overpotential, and dendrites-suppressed uniform growth of Li. Thanks to the homogeneous deposition, the oxidation treated electrodes delivered higher and more stable Coulombic efficiency (CE) than pristine electrodes (Fig. S6), consistent with the recent work where the oxidized brass mesh and copper foils delivered a higher and more stable CE than non-oxidized ones [42].

The Coulombic efficiency of Li plating/stripping on oxidation-treated electrodes was further evaluated and compared with the pristine electrodes. As shown in Fig. 5a, the growth of Li on ONiF exhibited lower nucleation potential and mass-transport overpotential than using pristine Ni foam. For ONiF, an excellent Coulombic efficiency remarkably steadied at 98.7% over 490 cycles was achieved (Fig. 5b), which was higher than the CE obtained previously [6,25,26,42–46]. In comparison, the pristine Ni foam presented a low and much fluctuated CE after 30 cycles. In some cycles the CE values with using Ni foam were above 100% (Fig. S7), which was because some dead lithium electrically reconnects to the electrode in the plating and becomes active again in the present stripping [7]. The lithium nucleation, growth and stripping on ONiF at the 50th to 100th and 400th cycle almost kept the same as shown in Fig. S6, proving the good stability of lithium storage with using oxidation-treated electrodes.

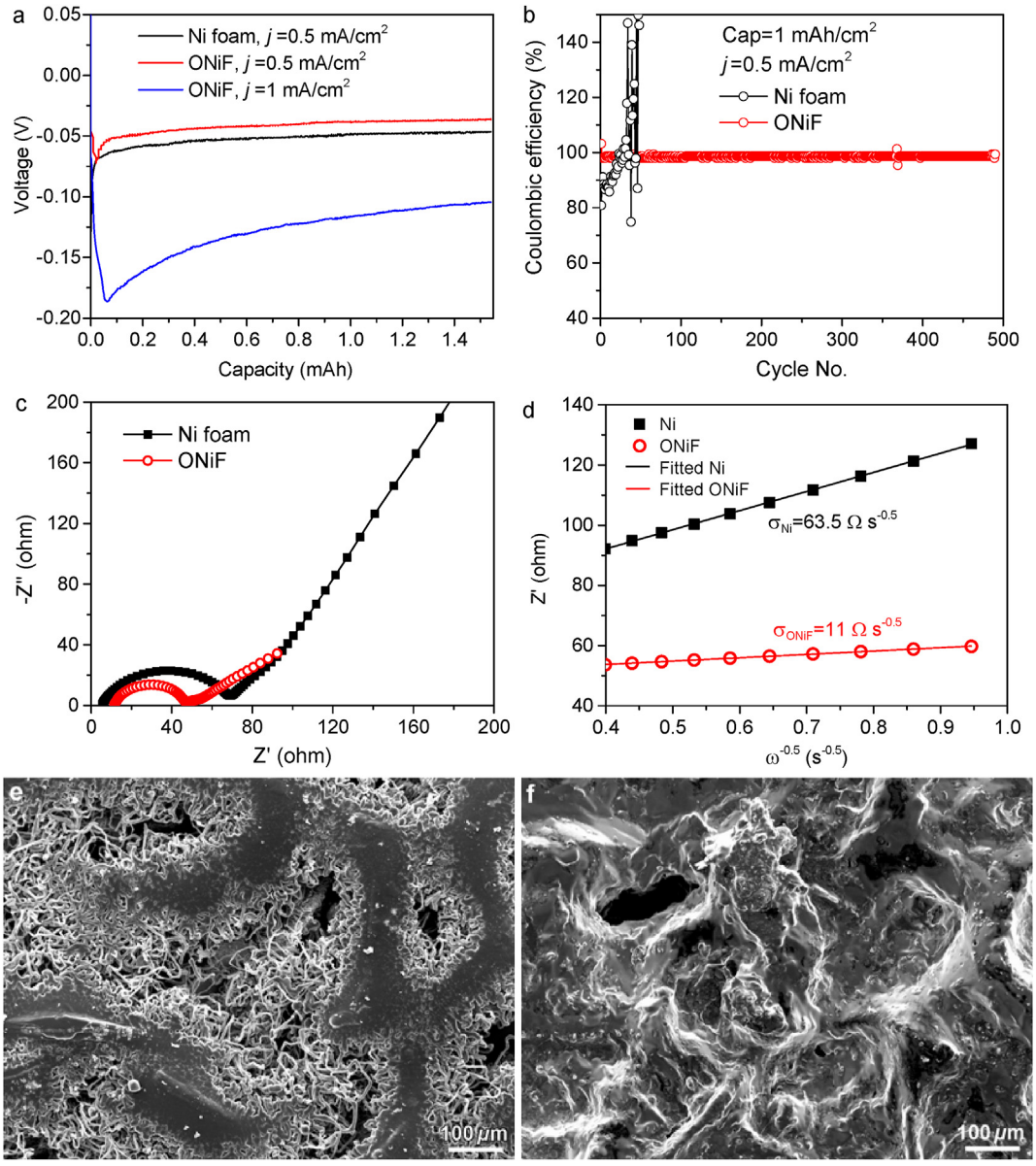

Fig. 5. (a) Voltage profile of Li deposition (1 mA h/cm^2) onto Ni and ONiF, (b) Coulombic efficiency of ONiF and non-oxidized Ni foam at 0.5 mA/cm^2 for 1 mA h/cm^2, (c) Nyquist plots of cells using ONiF and non-oxidized Ni foam before deposition of Li, (d) the relationship between Z′ and $\omega^{-0.5}$ at low frequencies. Microstructures of the plating of Li for 6 mA h/cm^2 at 1 mA/cm^2 in ether electrolyte onto different current collectors: (e) Ni foam, (f) ONiF.

The Nyquist plots in Fig. 5c proved that lithium growth had a lower interfacial charge-transfer resistance on ONiF than on non-oxidized Ni foam, which was consistent with the lower over-potential presented in the voltage profiles of galvanostatic Li plating. Fig. 5d shows the linear relationship between Z' and $\omega^{-0.5}$ in the low-frequency region. The Warburg coefficient σ for ONiF was much reduced in contrast to that for non-oxidized Ni (11 vs. 63.5 Ω/s$^{0.5}$), indicating a large increase of the diffusivity of ions. The ionic diffusivity still be kept higher for ONiF than Ni after the CE tests (Fig. S8). The lithium plating on ONiF and pristine Ni foam were also revealed as shown in Fig. 5 e-f. For a relatively high capacity of 6 mA h/cm^2, no dendrites were observed on ONiF. In contrast, the pores of Ni foam were fully filled with long and thick filaments.

The performances on Coulombic efficiency were further investigated under various current densities and capacities. For a capacity of 1 mA h/cm^2, at 1 mA/cm^2 the CE was retained at 98% for 350 cycles (Fig. 6a). When increasing the current density to 3 mA/cm^2, a high CE of ~96% was maintained after 300 cycles (Fig. 6b). In further raising the current density to 5 mA/cm^2, the CE ranged in 93%–95% from 1st to 100th cycle, and increased to 97% from 100th to 200th cycle (Fig. 6c). For the practical next-generation Li-metal batteries, a high capacity of over 3 mA h/cm^2 would be required. Thus the CE for a high capacity of 3 mA h cm^{-2} and 6 mA h cm^{-2} at 3 mA/cm^2 was evaluated. As shown in Fig. 6d and e, the high CE was kept at ~97% for over 140 cycles for 3 mA h/cm^2 and 98% for over 80 cycles for 6 mA h cm^{-2}. We also tested the CE of ONiF electrodes for areal capacities from 1 mA h/cm^2 to 8 mA h/cm^2 (Fig. 6f). Under these rigorous conditions, the CE remained at above 98.0%. The oxidized copper foam as current collectors also demonstrated good cyclic stability in Coulombic efficiency (Fig. S9). These results demonstrated that the surface oxidation of metal foam CCs can significantly improve the performances of lithium anodes with exceptional CE at ultrahigh areal capacities and current densities,

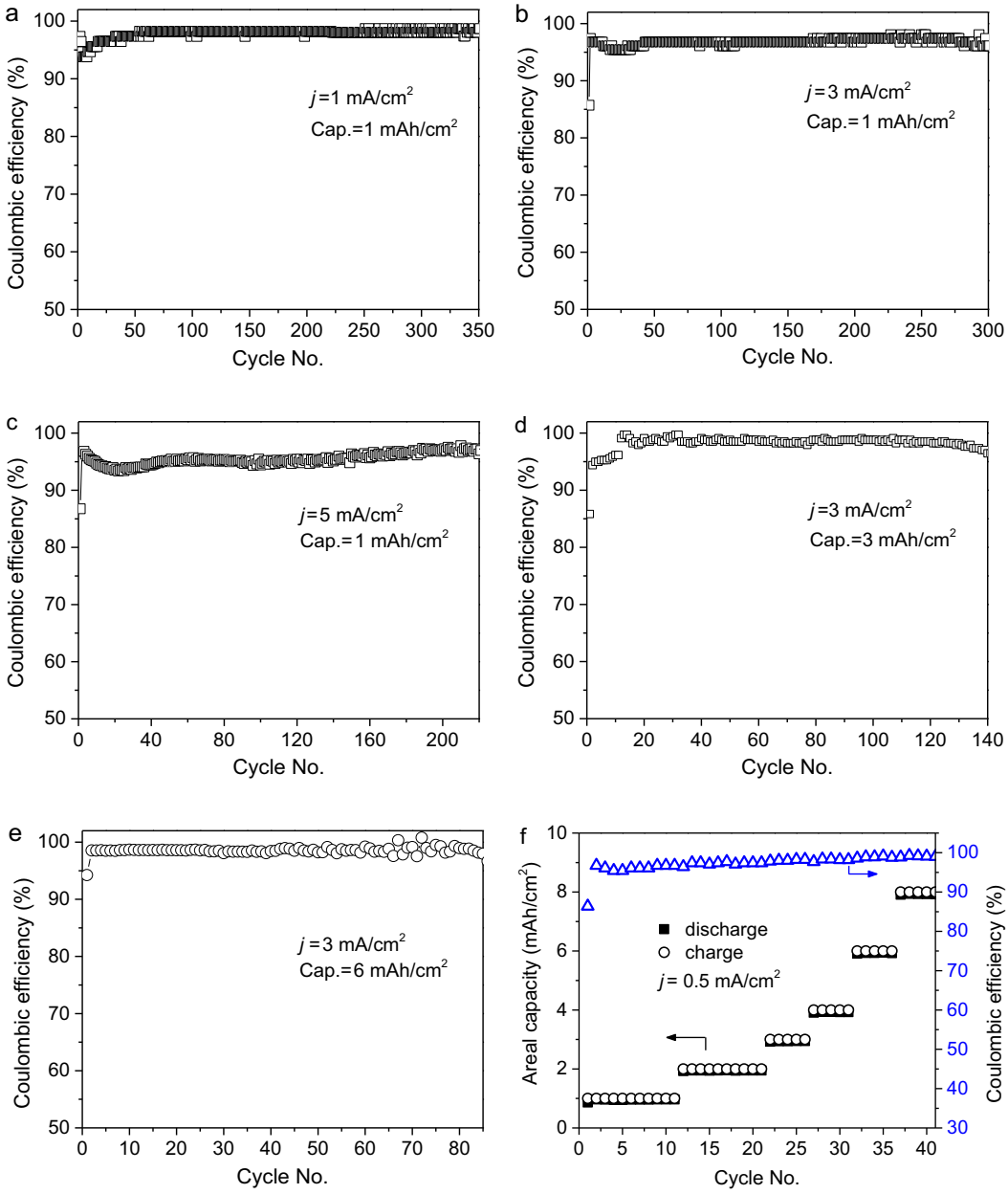

Fig. 6. Coulombic efficiency of ONiF with ether electrolyte: (a–c) at 1, 3 and 5 mA/cm^2 for 1 mA h/cm^2, (d, e) at 3 mA/cm^2 for 3 mA h/cm^2 and 6 mA h/cm^2, respectively, (f) at 0.5 mA/cm^2 for various capacities of from 1 mA h/cm^2 to 8 mA h/cm^2.

and the approach can be applied to broad metallic current collectors.

2.3. Solid electrolyte interphase formation and Li growth

It is known that the solid electrolyte interphase (SEI) film plays a critical role on the growth behavior of Li. The SEI films formed on the Ni and oxidized Ni foam were characterized by scanning electron microscopy (SEM). The Ni and oxidized Ni electrodes were cycled under 50 μA/cm^2 within potential of 1–0.001 V, then rinsed with 1, 2-Dimethoxyethane for several times to wash away the salts and dried in a glove box before tests. The pristine Ni had a clean surface (Fig. S10). It was found that a non-uniform SEI film with many thick domains of sub-micron size formed on pure Ni electrodes (Fig. S11). Similar non-uniform SEI films were also observed with using Cu as current collectors. In consistence with previous findings, elements of C, O, F and N were detected from the surface, indicating the existence of the species of lithium alkyl carbonates ($ROCO_2Li$), lithium fluorides (LiF), lithium alkoxides (ROLi), Li_xNO_y and so forth in the SEI [47]. The Energy dispersive X-ray spectroscopy (EDS) element mappings proved the formation of thick domains and the complete coverage of the Ni electrode with the inhomogeneous SEI films. In contrast, no thick SEI domains were clearly observed (Fig. S11h), reflecting a good uniformity of the SEI formed on the oxidized Ni.

To have more information, *ex-situ* transmission electron microscopy (TEM) was carried out to reveal the formation of SEI films. To preserve its pristine state, SEI was directly grown on Ni and oxidized Ni grids. Fig. 7a and Fig. S12 show the SEI films grown on the surface of Ni grid, demonstrating the non-uniform

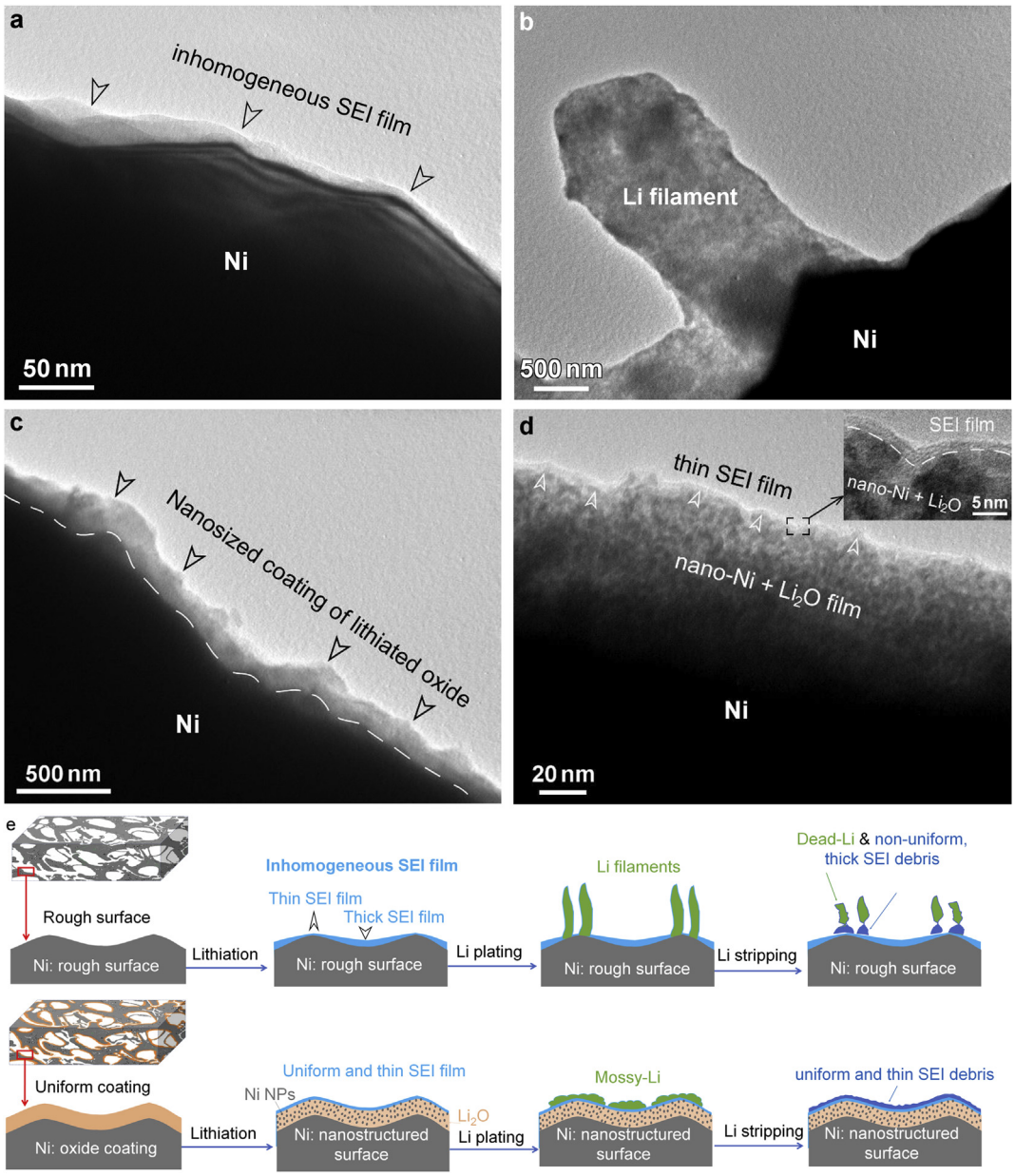

Fig. 7. (a) TEM image of SEI formed on pristine Ni surface, (b) TEM image of Li plating on pristine Ni surface at 10 μA/cm^2 for 10 μA h/cm^2, (c, d and the inset of d) TEM images of lithiated nickel oxide coating showing a uniform and thin SEI film formed on the nanocomposite coating composed of metal nanoparticles embedded in a Li_2O matrix, (e) schematic illustration of lithium plating and stripping processes on pristine metal current collectors (e.g. Ni) and the thermal oxidation treated current collectors.

SEI films containing thick and thin regions. The inhomogeneity of the SEI might be caused by the uneven localized current densities induced by the rough surfaces (Fig. S13). In consistence with previous results, the protrusions could induce the growth of Li filaments (Fig. 7b and Fig. S14). The lithiated oxide coating had an average thickness of 175 nm and was composed of lithium oxide (Li_2O) and metallic nanoparticles (Fig. 7c–d). In contrast, a thin and uniform SEI film can be observed on the outlayer of the lithiated oxide coating (inset of Fig. 7d), consistent with the SEM observations in terms of the uniformity of SEI. It was believed that the uniform and thin SEI film formed on the oxidized surface facilitated the diffusivity of ions, and the homogeneous growth of Li. The results also explained the reduced mass-transport overpotential during lithium plating.

On the basis of the above results, Fig. 7e schematically demonstrates the different growth behaviors of Li on oxide-modified metallic surface from the pristine metallic surface, which results in the differences in electrochemical performances. On pristine metallic current collectors, inhomogeneous SEI with various thicknesses formed, which can be originated from the uneven current densities induced by the rough surface. Recently Zhao et al. developed the polymer-based artificial SEI and found that too thick artificial SEI resulted in much poor cyclic stability [48]. To the same reason, it was believed that the non-uniform SEI that contains polymeric and distorted distribution of inorganic compounds (e.g. lithium alkyl carbonates [$ROCO_2Li$], lithium fluoride [LiF], lithium alkoxides [ROLi], Li_xNO_y) can also cause different diffusion of ions and uneven lithium growth at the interfaces, resulting in the formation of local thick and long Li filaments. It should be noted that, the current density applied was far below the critical current density in terms of characteristic time (the so-called Sand's time), implying that there might be other significant factors such as

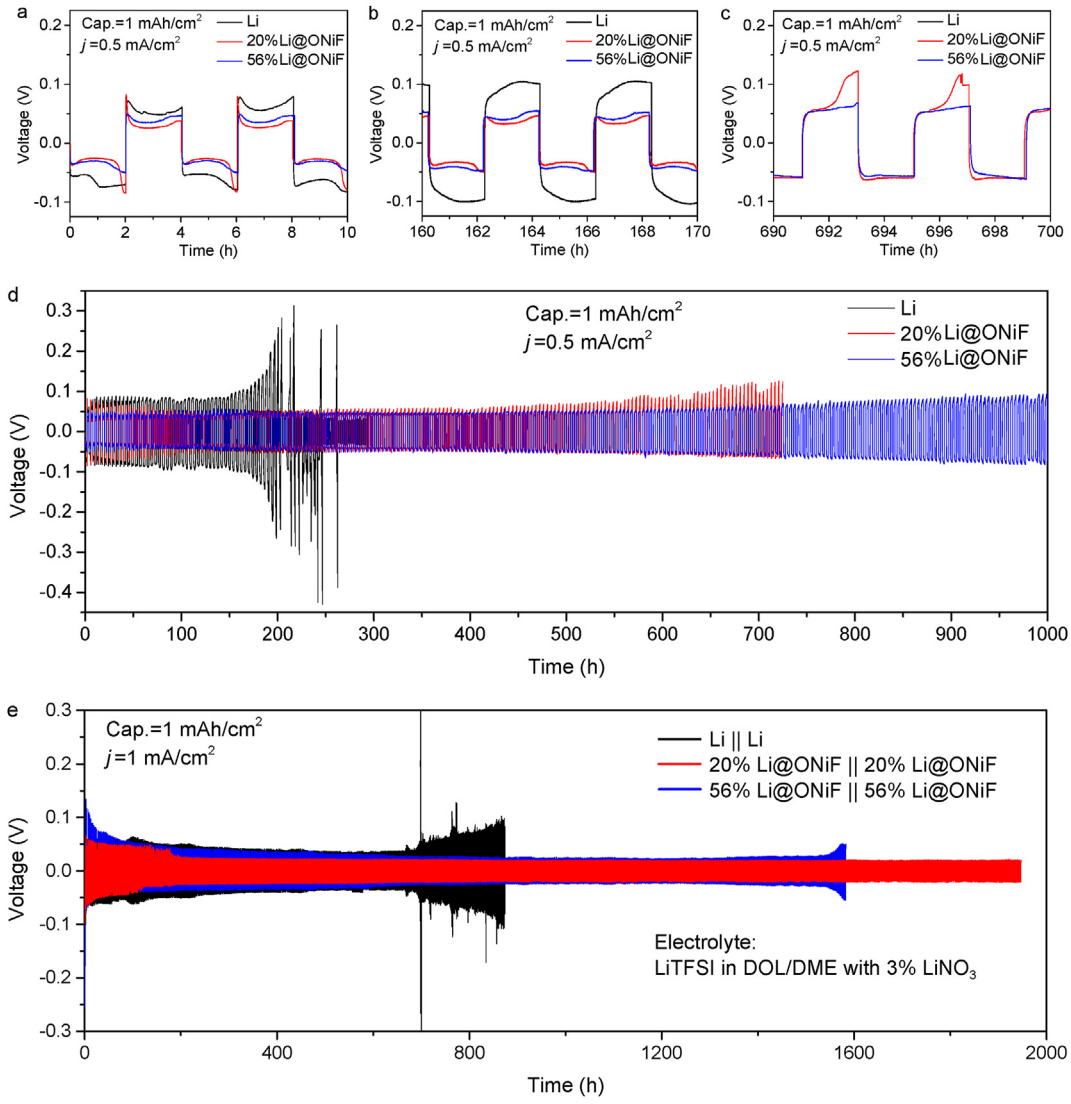

Fig. 8. (a–d) Voltage profiles of galvanostatic deposition and stripping of porous 20%Li@ONiF, non-porous 56%Li@ONiF and pure Li anodes in carbonate electrolyte, (e) galvanostatic deposition and stripping of symmetric cells in ether electrolyte.

surface geometry induced uneven SEI on the growth of dendritic Li [14]. In the stripping process, the roots of dendrites could strip first, leading to loss of electrical contact for the remaining parts that form as dead Li [7]. The unstable SEI debris and dead Li were the direct reasons causing increased voltage hysteresis and instable CE.

On oxidation-treated current collectors, the uniform oxide coating was converted to a nanostructure that was composed of Li_2O matrix and nanoporous metal. A thin and uniform SEI formed on outlayer of the modified surface, which increased the diffusivity of ions. Thanks to the tuned SEI, low nucleation energy and many nucleation sites from the Li_2O matrix, lithium uniformly grew at interfaces and kept good contact with the current collectors. Considering the observation of lithium dendrites on pure lithium surface that also provided many nucleation sites and low nucleation energy, in addition to the benefits from nucleation it was believed that the homogeneous and thin SEI was also crucial for guiding lithium growth. After lithium stripping, owing to the good electrical contact between Li and current collectors, very thin and uniform SEI debris and dead Li formed. Thus, a high, stable CE and low mass-transport overpotential were delivered for electrodes using oxidation-treated current collectors.

Regarding the increased diffusivity of ions, the following factors can be taken into account. First, the SEI film formed on modified current collectors was much thinner compared to using the pristine current collectors, introducing less resistance of ionic diffusion. Another factor was the nanostructure of the lithiated coating. The nanosized Li_2O formed in the lithiated coating could be in favor of the ionic transport. Different from bulk Li_2O, nanocrystalline Li_2O owned lower activation energy for local hopping of Li^+ in the outer layer and showed increased ionic conductivity [39]. In addition, the role of nanocrystalline Li_2O was also suggested to facilitate a Lewis-acid transport mechanism of Li^+ through the oxides [18].

2.4. Effects of porous and non-porous structures on electrochemical performances

Obviously, the content of Li influences the porosity and the specific capacity of the electrodes. The specific capacity (C_s) and volumetric capacity (C_v) of the composite Li anodes with a porous host can be generally formulated as below:

$$C_s = 3860\phi \quad (3)$$

$$C_v = \frac{3860\phi}{1-\phi}\rho_{porous} \quad (4)$$

where ϕ is the content (weight percentage) of Li in the composite, ρ_{porous} is the density of the porous host material. Eqs. (3) and (4) show that with increasing the content, the electrode capacities increases. Fig. S15 shows the theoretical specific and volumetric capacity of the Ni-foam constructed composite anodes as a function of the Li loading. Accordingly, the non-porous 56%Li@ONiF electrode owns much higher electrode capacities than porous 20% Li@ONiF.

To understand the effects of macroporous and non-porous structure on the electrochemical performances, the Li stripping/plating behaviors of the composites anodes were first investigated by half cells constructed with composite anodes as working electrodes and Li kept as the reference and counter electrodes. The commercial carbonate-based electrolytes were used. Fig. 8 a-d shows the voltage profiles of galvanostatic deposition and stripping of Li. In the initial few cycles, the porous 20%Li@ONiF composite electrodes exhibited lower voltage hysteresis (defined as the voltage difference between plating and stripping) than non-porous 56%Li@ONiF electrodes (51 mV vs. 64 mV). Both two composites electrodes had lower polarization compared with Li (117 mV). After 150 h, the voltage hysteresis of the porous and non-porous electrodes slightly increased to 66 mV and 80 mV, respectively (Fig. 8b). In contrast, the voltage hysteresis of pure Li anode increased quickly to 200 mV, followed with the aggravated voltage fluctuation and short circuit of the cells. Amazingly, both two composite electrodes exceeded more than 700 h. The non-porous composite electrodes exhibited the most stable voltage hysteresis over 1000 h (Fig. 8d). It was also noted that, the porous electrodes exhibited increased polarizations after 500 h during each later stage of stripping process as shown in Fig. 8c. The overpotential during plating or stripping process was mainly affected by the reaction kinetics and mass transport [49]. The lower voltage hysteresis for the non-porous electrodes than pure Li can be attributed to enhanced kinetics via the highly conductive three-dimensional Ni skeleton. In addition, porous electrodes had lower voltage hysteresis within 500 h compared with non-porous electrodes by virtue of the porous structure facilitated mass transport.

To further understand the causes for different cyclic stability, the microstructures of the electrodes after tests were investigated by scanning electron microscopy (SEM). Figs. S16a and b show the surface of pure Li electrode after galvanostatic deposition and stripping. A very thick dead lithium layer containing thick dendrites formed on the lithium and the thickness was 30–50 μm, causing increased mass-transport overpotential and voltage fluctuation. In contrast, on the surface of and inside the ligaments of porous composite electrodes, there were almost no dendrites found (Figs. S17a–c). However, a few of macropores were filled with accumulated SEI debris and thin dendritic dead lithium (Fig. S17d), which can cause the increased voltage hysteresis after 500 h cycling. For non-porous electrodes, there were no thick dendrites formed (Fig. S17e). The layer containing SEI debris and possible dead lithium had a thickness of around 9 μm (Fig. S17f), which was much thinner than that formed on pure Li anode. The above results demonstrated that the porous current collector effectively reduced Li dendrites and SEI debris layer. Moreover, although both porous and non-porous electrodes were enhanced by the Ni framework, the porous electrodes had larger surface area exposed to the electrolyte in contrast to the non-porous electrodes, providing more area for the formation of SEI debris and leading to shorter stability in comparison with the non-porous electrodes. In summary, the geometrical structure, conductive network, unstable SEI formation all resulted in the different cyclic stabilities for porous and non-porous composites electrodes.

The galvanostatic deposition and stripping behaviors of lithium in ether-based electrolyte were evaluated in symmetric cells. As shown in Fig. 8e, the voltage hysteresis of all the electrodes gradually decreased in the early stage (0–200 h), and then tended to become steady. The voltage hysteresis of the composite anodes was smaller and turned into steady state more quickly than that of pristine Li anodes. The composite anodes kept steady for more than 1500 h. In contrast, the voltage hysteresis of Li anodes became fluctuated after 670 h, and then increased dramatically. The 20% Li@ONiF anodes exhibited the lowest voltage hysteresis of 36 mV and the 56%Li@ONiF anodes got a low voltage hysteresis of 40 mV, competent with other reported porous hosts. The non-porous 56% Li@ONiF anodes steadily cycled for over 1500 h and then went into voltage fluctuation. The porous 20%Li@ONiF anodes steadily cycled for over 1900 h. Thus, the above results show that in the ether-based electrolyte the porous electrodes performed better stabilities and lower overpotential than the non-porous electrodes. After cyclic tests, the electrodes were examined with SEM. It was observed that there were much less lithium filaments and SEI debris formed compared with using carbonate electrolyte (Fig. S18). In carbonate electrolyte, the formation of thick SEI debris seriously consumed electrolytes and increased the mass-transfer resistance, thus causing high polarization and instability. As the porous electrodes had larger surface area than the non-porous electrodes, more SEI debris can form on porous electrodes in carbonate electrolyte (Fig. S17), resulting in faster depletion of electrolyte, higher mass-transfer resistance, and shorter stable Li plating/stripping in carbonate electrolyte. But the ether electrolyte was in favor of dendrite-free lithium deposition, thus SEI debris accumulated less and at slower rate (Fig. S18). Thus, in ether electrolyte, the porous structure of 20%Li@ONiF anodes was beneficial for mass transport and delayed Sand's time, leading to lower polarization and better stability than non-porous electrodes.

The ratio of cycling capacity to the total capacity of the electrode in terms of the cyclic stability is a key influencing factor and significant for practical applications. Considering the ratio was only ~2.8% for 20%Li@ONiF anode because of much excessive lithium not utilized, we reduced the lithium loading to a capacity of around 10 mA h/cm^2 on oxidized copper foam, and then measured the cyclic stability at 0.5 mA/cm^2 for 1 mA h/cm^2 that was corresponding to ~10% of active lithium in the electrode. As shown in Fig. S19, the low-Li-loading composite electrode demonstrated much better stability, longer life, and lower voltage hysteresis in comparison with lithium anode (450 μm) that only had a cycling capacity of ~1% in Li electrode. It demonstrated that the composite anodes constructed with oxidation-treated current collectors much enhanced the electrochemical performances and would work in practical conditions.

The advantages of ONiF constructed composite anodes and the effects of porous and non-porous structure on electrochemical performances can be also reflected by the full-cell performances. Lithium titanium oxide, $Li_4Ti_5O_{12}$ (LTO) was selected for the full-cell configurations due to its excellent rate performances under high loadings. As show in Fig. 9a, the LTO cathodes paired with the composite anodes, exhibited higher capacity than those with pure Li. Especially at high rates from 0.5C to 10C, the composite anodes outperformed pure lithium to a great extent. For example, at 1C the capacities of 142 mA h/g, 125 mA h/g and 105 mA h/g were obtained for 20%Li@ONiF, 56%Li@ONiF and pure lithium anodes, respectively. Moreover, the porous anodes illustrated significant improvements in capacities at various rates compared to non-porous anodes. The voltage profiles at different rates intimated possible reasons. As shown in Fig. 9b and c, the polarizations for 20%Li@ONiF anodes

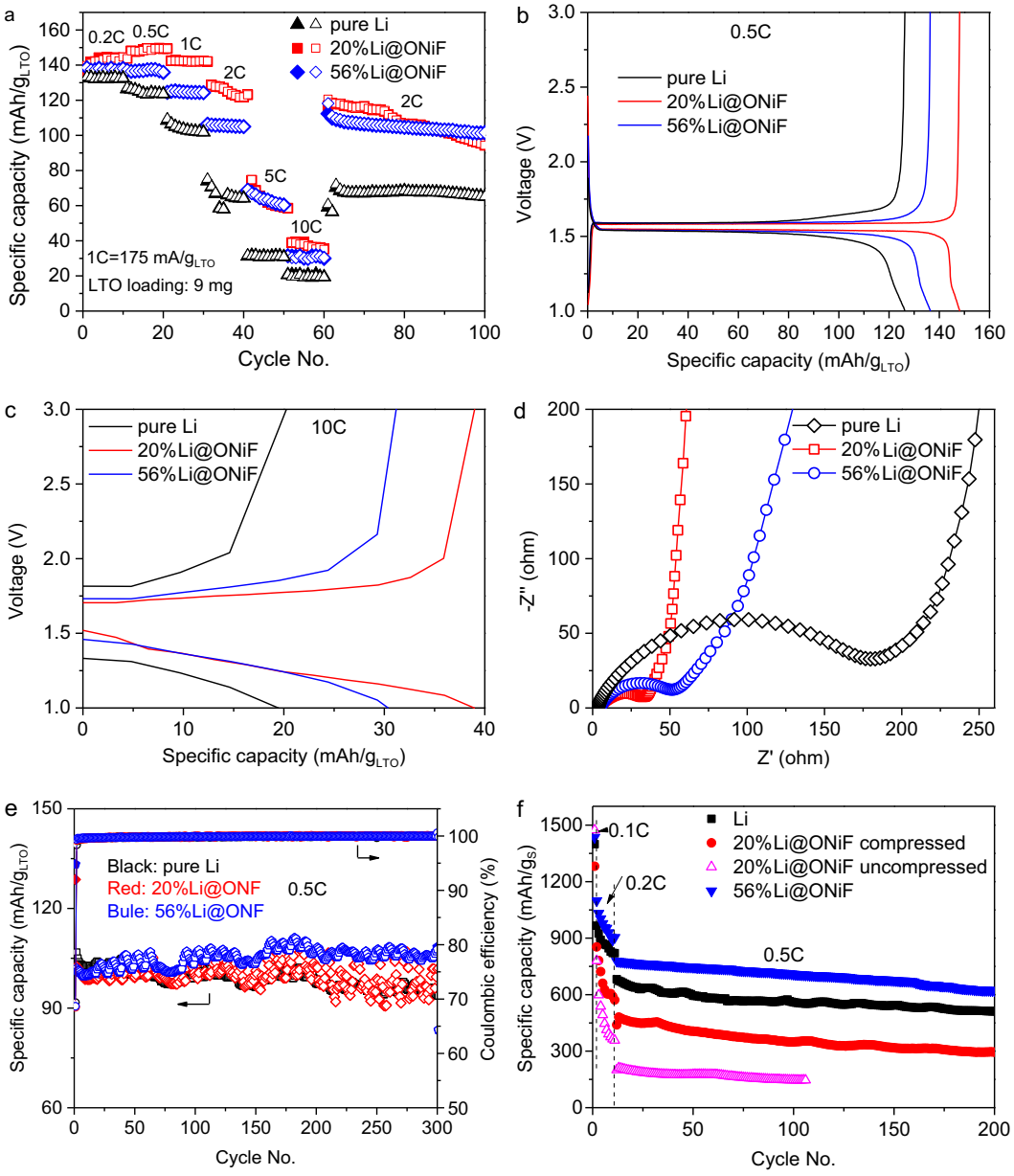

Fig. 9. (a) Galvanostatic rate performances of LTO electrodes paired with 20%Li@ONiF, 56%Li@ONiF, and pure Li with electrolyte of $LiPF_6$ in EC/DEC; (b, c) Voltage profiles at 0.5C and 10C, (d) Nyquist plots of batteries of LTO paired with the three electrodes; (e) Galvanostatic cyclic performances of LTO electrodes paired with 20%Li@ONiF, 56%Li@ONiF and pure Li with ether-based electrolyte; (f) cyclic performances of S electrodes paired with 20%Li@ONiF, compressed 20%Li@ONiF, 56%Li@ONiF and pure Li.

were lower than those of 56%Li@ONiF and pure lithium anodes, especially under high current density such as 10C. The reduced overpotential for porous anodes was ascribed to either the faster mass transport facilitated by the porous structures, or the lower activation overpotential enhanced by the intimate contact between Li and Ni. The Nyquist plots in Fig. 9d revealed that the composite anodes had lower charge transfer resistances at interfaces than pure lithium, while 20%Li@ONiF had the lowest charge transfer resistances. It indicated that the porous structure of the composite anodes can significantly enhance the reaction kinetics. The lower interfacial charge transfer resistance of porous anode compared with non-porous anodes can be attributed to the higher surface area.

In further analysis, the cyclic performances of full-cell batteries in ether-based electrolyte were investigated using composite anodes paired with LTO and sulfur electrodes. As shown in Fig. 9e, all LTO electrodes delivered similar performances at 0.5C for the first 150 cycles. After that, the capacity for using non-porous composite anodes slightly increased. In contrast, using pure Li the capacity showed obvious decay. The porous composite anodes gradually exhibited large fluctuation from 150th to 300th cycles, which was caused by the consumption of electrolyte and lithium, and repeated formation of SEI debris. Compared with the non-porous electrodes, the porous electrode having high surface area and pore volume consumed more electrolyte as well. Fig. 9f shows the electrochemical performances of Li–S batteries using the composite anodes and Li. The non-porous composite anodes exhibited the highest specific capacity among them. Compared with the pristine lithium anode, the enhanced capacity of non-porous composite anodes was attributed to the reduced charge-transfer resistances (Fig. S20). However, with using the porous composite anodes the sulfur cathodes delivered the lowest

capacity. It was resulted from the macropores that filled with more electrolyte, in which more polysulfides can dissolve. It was also proved a higher capacity can be obtained by compressing the porous anode to reduce the porosity and thus the insufficiency of electrolyte.

The above results demonstrated the large influences of macroporous and non-porous structure on the electrochemical performances. Balancing the porosity and capacity was tricky. Although macroporous electrodes exhibited better plating and stripping performances than non-porous electrodes, practically the porous electrodes needed more electrolyte that compromises the battery capacity, making it even lower than using non-porous electrodes. The high surface area of porous electrodes additionally made higher consumption of electrolyte for repeated SEI formation especially in carbonate electrolyte. The lowered porosity can be rather significant for Li–S batteries due to the dissolution of polysulfides into the electrolyte. Electrodes with reduced macroporous to nanoporous could balance the fast mass transport and high capacity for designing high-energy density and high-power batteries.

It should be also mentioned that construction of a non-porous anode with a low lithium loading and a reasonable electrode thickness (such as 10–50 μm thick) for practical applications is crucial and needs engineering thin porous current collectors with suitable pore sizes. In addition, there might be influences of reducing the pore sizes, thickness of the electrodes (down to 10–50 μm thick) and lithium loadings on the electrochemical performances (including half-cell and full-cell performances), which might be interesting for future investigations.

3. Conclusion

In conclusion, the effect of lithiophilic oxide coating modified metal foam current collectors by a facile thermal oxidation process on the performances of lithium anode was investigated. In comparison with pristine metal foam current collectors, the surface oxidation treatment facilitated the formation of uniform SEI and even lithium deposition. The diffusivity of ions were much increased with using oxides modified current collectors. It exhibited lower energy barrier for the lithium nucleation and growth, and higher reaction rate when using oxides-modified current collectors than pristine current collectors. A higher Coulombic efficiency and better stability were delivered with modified current collectors than the pristine ones. A remarkable Coulombic efficiency steady at 98.7% over 490 cycles for ONiF was obtained.

The composite anodes show lower overpotential, longer lifetime, and better rate performances in the full-cell batteries than pure Li anodes. In addition, balancing the porosity and capacity was tricky. The porous composite anodes achieved lower overpotential during plating/stripping and better rate performances. However, the non-porous composite electrodes surpassed the macroporous electrodes in terms of the stability and overall capacity, in particular for the Li–S batteries as porous composite anodes require more electrolyte that can dissolve active species.

Our research findings can be also useful for designing other metal anodes (e.g. Zn, Na and K) with using metallic and non-metallic porous host materials (e.g. porous copper, porous carbon, graphene, carbon nanotube and nanofibers).

Credit author statement

Liqiang Lu: Conceptualization, Data curation, Investigation, Methodology, Formal analysis, Writing - original draft. **Yutao Pei:** Funding acquisition, Conceptualization, Formal analysis, Writing - review & editing, Supervision.

Declaration of competing interest

The authors declare that they have no known competing financial interests or personal relationships that could have appeared to influence the work reported in this paper.

Appendix A. Supplementary data

Supplementary data to this article can be found online at https://doi.org/10.1016/j.mtener.2021.100748.

References

[1] D. Larcher, J.M. Tarascon, Towards greener and more sustainable batteries for electrical energy storage, Nat. Chem. 7 (1) (2015) 19–29.
[2] B. Dunn, H. Kamath, J.M. Tarascon, Electrical energy storage for the grid: a battery of choices, Science 334 (6058) (2011) 928–935.
[3] J. Liu, Z. Bao, Y. Cui, E.J. Dufek, J.B. Goodenough, P. Khalifah, Q. Li, B.Y. Liaw, P. Liu, A. Manthiram, Y.S. Meng, V.R. Subramanian, M.F. Toney, V.V. Viswanathan, M.S. Whittingham, J. Xiao, W. Xu, J. Yang, X.-Q. Yang, J.-G. Zhang, Pathways for practical high-energy long-cycling lithium metal batteries, Nat. Energy 4 (3) (2019) 180–186.
[4] H. Yang, C. Guo, A. Naveed, J. Lei, J. Yang, Y. Nuli, J. Wang, Recent progress and perspective on lithium metal anode protection, Energy Storage Mater 14 (2018) 199–221.
[5] M. Yan, W.-P. Wang, Y.-X. Yin, L.-J. Wan, Y.-G. Guo, Interfacial design for lithium–sulfur batteries: from liquid to solid, Energy 1 (1) (2019) 100002.
[6] Q. Li, S. Zhu, Y. Lu, 3D porous Cu current collector/Li-metal composite anode for stable lithium-metal batteries, Adv. Funct. Mater. 27 (18) (2017) 1606422.
[7] J. Xie, J. Wang, H.R. Lee, K. Yan, Y. Li, F. Shi, W. Huang, A. Pei, G. Chen, R. Subbaraman, J. Christensen, Y. Cui, Engineering stable interfaces for three-dimensional lithium metal anodes, Sci. Adv. 4 (7) (2018), eaat5168.
[8] H. Wang, Y. Li, Y. Li, Y. Liu, D. Lin, C. Zhu, G. Chen, A. Yang, K. Yan, H. Chen, Y. Zhu, J. Li, J. Xie, J. Xu, Z. Zhang, R. Vila, A. Pei, K. Wang, Y. Cui, Wrinkled graphene cages as hosts for high-capacity Li metal anodes shown by cryogenic electron microscopy, Nano Lett. 19 (2) (2019) 1326–1335.
[9] N. Kränzlin, M. Niederberger, Controlled fabrication of porous metals from the nanometer to the macroscopic scale, Mater. Horiz. 2 (4) (2015) 359–377.
[10] C. Cui, C. Yang, N. Eidson, J. Chen, F. Han, L. Chen, C. Luo, P.F. Wang, X. Fan, C. Wang, A highly reversible, dendrite-free lithium metal anode enabled by a lithium-fluoride-enriched interphase, Adv. Mater. 32 (12) (2020), e1906427.
[11] X.B. Cheng, R. Zhang, C.Z. Zhao, F. Wei, J.G. Zhang, Q. Zhang, A review of solid electrolyte interphases on lithium metal anode, Adv. Sci. 3 (3) (2016) 1500213.
[12] H. Chen, A. Pei, D. Lin, J. Xie, A. Yang, J. Xu, K. Lin, J. Wang, H. Wang, F. Shi, D. Boyle, Y. Cui, Uniform high ionic conducting lithium sulfide protection layer for stable lithium metal anode, Adv. Energy Mater. 9 (22) (2019) 1900858.
[13] S. Li, Q. Liu, X. Wang, Q. Wu, L. Fan, W. Zhang, Z. Shen, L. Wang, M. Ling, Y. Lu, Constructing a phosphating–nitriding interface for practically used lithium metal anode, ACS Mater. Lett. 2 (1) (2019) 1–8.
[14] D. Lin, Y. Liu, Y. Cui, Reviving the lithium metal anode for high-energy batteries, Nat. Nanotechnol. 12 (3) (2017) 194–206.
[15] Y.Z. Li, Y.B. Li, A. Pei, K. Yan, Y.M. Sun, C.-L. Wu, L.-M. Joubert, R. Chin, A.L. Koh, Y. Yu, J. Perrino, B. Butz, S. Chu, Y. Cui, Atomic structure of sensitive battery materials and interfaces revealed by cryo–electron microscopy, Science 358 (2017) 506–510.
[16] D. Aurbach, Y. Ein-Ely, A. Zaban, The surface chemistry of lithium electrodes in alkyl carbonate solutions, J. Electrochem. Soc. 141 (1994) L1.
[17] E. Peled, D. Golodnitsky, G. Ardel, Advanced model for solid electrolyte interphase electrodes in liquid and polymer electrolytes, J. Electrochem. Soc. 144 (1997) L208.
[18] W. Huang, D.T. Boyle, Y. Li, Y. Li, A. Pei, H. Chen, Y. Cui, Nanostructural and electrochemical evolution of the solid-electrolyte interphase on CuO nanowires revealed by cryogenic-electron microscopy and impedance spectroscopy, ACS Nano 13 (1) (2019) 737–744.
[19] P. Lu, C. Li, E.W. Schneider, S.J. Harris, Chemistry, impedance, and morphology evolution in solid electrolyte interphase films during formation in lithium ion batteries, J. Phys. Chem. C 118 (2) (2014) 896–903.
[20] M. Nie, D.P. Abraham, Y. Chen, A. Bose, B.L. Lucht, Silicon solid electrolyte interphase (SEI) of lithium ion battery characterized by microscopy and spectroscopy, J. Phys. Chem. C 117 (26) (2013) 13403–13412.
[21] L. Wang, A. Menakath, F. Han, Y. Wang, P.Y. Zavalij, K.J. Gaskell, O. Borodin, D. Iuga, S.P. Brown, C. Wang, K. Xu, B.W. Eichhorn, Identifying the components of the solid-electrolyte interphase in Li-ion batteries, Nat. Chem. 11 (9) (2019) 789–796.
[22] J. Zhang, R. Wang, X. Yang, W. Lu, X. Wu, X. Wang, H. Li, L. Chen, Direct observation of inhomogeneous solid electrolyte interphase on MnO anode with atomic force microscopy and spectroscopy, Nano Lett. 12 (4) (2012) 2153–2157.
[23] K. Yan, Z. Lu, H.-W. Lee, F. Xiong, P.-C. Hsu, Y. Li, J. Zhao, S. Chu, Y. Cui, Selective deposition and stable encapsulation of lithium through heterogeneous seeded growth, Nat. Energy 1 (3) (2016) 16010.

[24] C. Sun, Y. Li, J. Jin, J. Yang, Z. Wen, ZnO nanoarray-modified nickel foam as a lithiophilic skeleton to regulate lithium deposition for lithium-metal batteries, J. Mater. Chem. 7 (13) (2019) 7752–7759.
[25] C.P. Yang, Y.X. Yin, S.F. Zhang, N.W. Li, Y.G. Guo, Accommodating lithium into 3D current collectors with a submicron skeleton towards long-life lithium metal anodes, Nat. Commun. 6 (2015) 8058.
[26] Z. Zhang, X. Xu, S. Wang, Z. Peng, M. Liu, J. Zhou, C. Shen, D. Wang, Li_2O-reinforced Cu nanoclusters as porous structure for dendrite-free and long-lifespan lithium metal anode, ACS Appl. Mater. Inter. 8 (40) (2016) 26801–26808.
[27] G. Huang, P. Guo, J. Wang, S. Chen, J. Liang, R. Tao, S. Tang, X. Zhang, S. Cheng, Y.-C. Cao, S. Dai, Lithiophilic V_2O_5 nanobelt arrays decorated 3D framework hosts for highly stable composite lithium metal anodes, Chem. Eng. J. 384 (15) (2020) 123313.
[28] G. Huang, S. Chen, P. Guo, R. Tao, K. Jie, B. Liu, X. Zhang, J. Liang, Y.-C. Cao, In situ constructing lithiophilic NiFx nanosheets on Ni foam current collector for stable lithium metal anode via a succinct fluorination strategy, Chem. Eng. J. 395 (1) (2020) 125122.
[29] N. Phattharasupakun, J. Wutthiprom, S. Duangdangchote, M. Sawangphruk, A 3D free-standing lithiophilic silver nanowire aerogel for lithium metal batteries without lithium dendrites and volume expansion: in operando X-ray diffraction, Chem. Commun. 55 (40) (2019) 5689–5692.
[30] Z. Liang, D. Lin, J. Zhao, Z. Lu, Y. Liu, C. Liu, Y. Lu, H. Wang, K. Yan, X. Tao, Y. Cui, Composite lithium metal anode by melt infusion of lithium into a 3D conducting scaffold with lithiophilic coating, Proc. Natl. Acad. Sci. U. S. A 113 (11) (2016) 2862–2867.
[31] H. Ye, S. Xin, Y.X. Yin, J.Y. Li, Y.G. Guo, L.J. Wan, Stable Li Plating/stripping electrochemistry realized by a hybrid Li reservoir in spherical carbon granules with 3D conducting skeletons, J. Am. Chem. Soc. 139 (16) (2017) 5916–5922.
[32] F. Pei, A. Fu, W. Ye, J. Peng, X. Fang, M.S. Wang, N. Zheng, Robust lithium metal anodes realized by lithiophilic 3D porous current collectors for constructing high-energy lithium-sulfur batteries, ACS Nano 13 (7) (2019) 8337–8346.
[33] L. Chen, H. Chen, Z. Wang, X. Gong, X. Chen, M. Wang, S. Jiao, Self-supporting lithiophilic N-doped carbon rod array for dendrite-free lithium metal anode, Chem. Eng. J. 363 (2019) 270–277.
[34] S.A. Krat, A.S. Popkov, Y.M. Gasparyan, A.A. Pisarev, P. Fiflis, M. Szott, M. Christenson, K. Kalathiparambil, D.N. Ruzic, Wetting properties of liquid lithium on lithium compounds, Fus. Eng. Des. 117 (2017) 199–203.
[35] S.-S. Chi, Y. Liu, W.-L. Song, L.-Z. Fan, Q. Zhang, Prestoring lithium into stable 3D nickel foam host as dendrite-free lithium metal anode, Adv. Funct. Mater. 27 (24) (2017) 1700348.
[36] L. Qin, H. Xu, D. Wang, J. Zhu, J. Chen, W. Zhang, P. Zhang, Y. Zhang, W. Tian, Z. Sun, Fabrication of lithiophilic copper foam with interfacial modulation toward high-rate lithium metal anodes, ACS Appl. Mater. Inter. 10 (33) (2018) 27764–27770.
[37] Y. Zhang, W. Luo, C. Wang, Y. Li, C. Chen, J. Song, J. Dai, E.M. Hitz, S. Xu, C. Yang, Y. Wang, L. Hu, High-capacity, low-tortuosity, and channel-guided lithium metal anode, Proc. Natl. Acad. Sci. U.S.A. 114 (14) (2017) 3584–3589.
[38] Y.S. Hu, Y.G. Guo, W. Sigle, S. Hore, P. Balaya, J. Maier, Electrochemical lithiation synthesis of nanoporous materials with superior catalytic and capacitive activity, Nat. Mater. 5 (9) (2006) 713–717.
[39] M.M. Islam, T. Bredow, Density functional theory study for the stability and ionic conductivity of Li_2O surfaces, J. Phys. Chem. C 113 (2) (2009) 672–676.
[40] L. Lu, F. Pei, T. Abeln, Y. Pei, Tailoring three-dimensional interconnected nanoporous graphene micro/nano-foams for lithium-sulfur batteries, Carbon 157 (2020) 437–447.
[41] P. Bai, J. Li, F.R. Brushett, M.Z. Bazant, Transition of lithium growth mechanisms in liquid electrolytes, Energy Environ. Sci. 9 (10) (2016) 3221–3229.
[42] S. Huang, W. Zhang, H. Ming, G. Cao, L.Z. Fan, H. Zhang, Chemical energy release driven lithiophilic layer on 1 m(2) commercial brass mesh toward highly stable lithium metal batteries, Nano Lett. 19 (3) (2019) 1832–1837.
[43] K. Xie, W. Wei, K. Yuan, W. Lu, M. Guo, Z. Li, Q. Song, X. Liu, J.-G. Wang, C. Shen, Toward dendrite-free lithium deposition via structural and interfacial synergistic effects of 3D graphene@Ni scaffold, ACS Appl. Mater. Inter. 8 (39) (2016) 26091–26097.
[44] X.B. Cheng, T.Z. Hou, R. Zhang, H.J. Peng, C.Z. Zhao, J.Q. Huang, Q. Zhang, Dendrite-free lithium deposition induced by uniformly distributed lithium ions for efficient lithium metal batteries, Adv. Mater. 28 (15) (2016) 2888–2895.
[45] X. Ke, Y. Liang, L. Ou, H. Liu, Y. Chen, W. Wu, Y. Cheng, Z. Guo, Y. Lai, P. Liu, Z. Shi, Surface engineering of commercial Ni foams for stable Li metal anodes, Energy Storage Mater 23 (2019) 547–555.
[46] D. Zhang, A. Dai, M. Wu, K. Shen, T. Xiao, G. Hou, J. Lu, Y. Tang, Lithiophilic 3D porous CuZn current collector for stable lithium metal batteries, ACS Energy Lett 5 (1) (2019) 180–186.
[47] D. Aurbach, E. Pollak, R. Elazari, G. Salitra, C.S. Kelley, J. Affinito, On the surface chemical aspects of very high energy density, rechargeable Li–sulfur batteries, J. Electrochem. Soc. 156 (8) (2009) A694–A702.
[48] Y. Zhao, D. Wang, Y. Gao, T. Chen, Q. Huang, D. Wang, Stable Li metal anode by a polyvinyl alcohol protection layer via modifying solid-electrolyte interphase layer, Nano Energy 64 (2019) 10393.
[49] A. Pei, G. Zheng, F. Shi, Y. Li, Y. Cui, Nanoscale nucleation and growth of electrodeposited lithium metal, Nano Lett. 17 (2) (2017) 1132–1139.